Evaluation of the ship resistance using computational fluid dynamics at various Froude numbers

Aries Sulisetyono[1*] and M. H. N. Alifrananda[2]
{sulisea@na.its.ac.id[1], mhafiznurwahyu@gmail.com[2]}

[1,2]Department of Naval Architecture, Institut Teknologi Sepuluh Nopember
Kampus ITS Sukolilo Surabaya

Abstract. In the ship design stage, the accuracy of the evaluation of ship resistance using a computational method that closely matches the findings of model tests is essential. This paper presents the computing method employed by the Reynolds Average Navier Stoke equation to compute the ship's hull resistance of the model DTMB 5415. The Volume of Fluid (VOF) feature of NUMECA software is utilized to capture the incompressible free surface flow over the ship's wetted surface area at three different speeds. The standard k–ω STT turbulence model is employed. A hybrid grid is generated using the CFD grid generator for the full boundary condition problem. The simulation setup conditions correspond to those for which previously published experimental results were obtained. The numerical simulation results presented agree with the available experimental results.

Keywords: DTMB 5415 ship, ship resistance, computational fluid dynamic

1 Introduction

Predicting the the wave-making resistance requires a comprehensive understanding of the wave patterns created by ships navigating through calm water. The energy radiated and contained by a ship's waves must be dispersed into the fluid surrounding the hull. The ship encounters a force that resists its forward speed; this force is wave-making resistance, which is caused by the ship's wake following the body. The ship suffers a force that resists its forward speed; this is the wave-making resistance component of the ship's resistance caused to wake after the body. In simulating the wave forming resistance problem under the assumption of ideal flow, the Rankine source approach is recognized as the most common technique [1,2]. In accordance with the so-called multiple model solution given by Dawson [3], it is possible to successfully include free surface boundary conditions in the simulation process. This model was used in many practical situations, and it has been improved in many ways to explain the nonlinear behavior of free surfaces [4].

Taking into account free surface effects, the computer program for modeling viscous flow may simulate the turbulent flow across a ship's wetted surface. This algorithm is also capable of giving reasonably accurate results for flow field and vessel resistance. In addition, the code is required for analyzing certain flow characteristics, for instance the point of flow separation towards the stern of a ship, for which the flow field patterns may only be reproduced using a real fluid approach. Numerical procedure relies on discretization, including the finite volume method,

ICSEDTI 2022, October 11-13, Tanjungpinang, Indonesia

DOI 10.4108/eai.11-10-2022.2326428

are utilized to handle fluid-related problems. Depending on the conformance of the computational mesh to the form or location of the free surface, a viscous flow program can be used to model free surface problems such as the formation of waves. Interface tracking methods, such as moving mesh [5,6], and interface capture methods, such as fluid volume methods [7,8], are thus the two most common approaches to calculating free surfaces. Previously, the mesh moved across a set Eulerian grid to trace flow patterns of free surface over the hull surface. The mesh contains solely water-involved domains, with the free surfaces being the upper bounds of the fluid domain and being defined like a part of the answer. The method is applicable to issues with shifting boundary conditions, although additional treatment is needed to model significant deformation problems. Fluids of water and air are recognized as effective properties in the modeling of the interfacial capture method. By solving an additional transport equation, the location of the free surface can be determined, as the number grid is immobile in space.

This article examines a free surface flow over the DTMB 5415 model for Froude numbers of 0.1, 0.28, and 0.41 utilizing the NUMECA code. The frictional and pressure resistances of the ship model are calculated numerically using the finite volume approach. The simulation assumes flow stability and uses the classic k-ω SST turbulence flow model as given in [9]. The numerical findings are contrasted with the experimental data that have been published in [10].

2 Methodology

2.1 Ship Hull Dimensions

Figure 1 shows the hull design of the model DTMB 5415, which is a hull model for a United States battleship. This model has an unusual bow shape, in which there is a bulbous bow model that is below the baseline of the ship. This ship is a displacement ship and is often used as a study for the development of a prototype hull model, so that the DTMB 5415 hull model is worthy of being used as a model for validation of numerical simulation results, considering the frequent use of this hull model as study material in many hydrodynamic laboratories in the world. The principal dimensions of the DTMB 5415 model test are explained in Table 1, which considers the David Taylor Model Basin model tests (DTMB). The ITTC published tank towing test results for this hull model in three variations of the Froude number, namely 0.1, 0.28, and 0.41 [10].

Table 1. Main dimensions of DTMB 5415 model [15]

Parameter	Model Scale	Units
Length Between Perependicular (LPP)	5.720	m
Breadth (B)	0.76	m
Draught (T)	0.248	m
Displacement (∇)	0.549	tons
Wetted Surface Area (WSA)	4.786	m^2
Block coefficient	0.5	

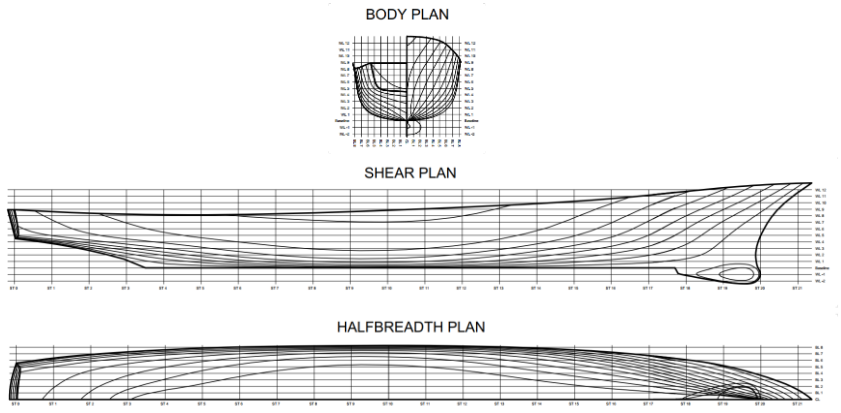

Fig. 1. DTMB 5415 Lines plan.

2.2 Mathematical model

The CFD code utilized the Reynolds-averaged Navier Stokes (RANS) equations under the assumption of incompressible and unsteady flow, whereas the k – ω SST model is used to solve the turbulence. Transport equations are spatially discretized by means of the finite volume approach. In order to build nonoverlapping control volumes, the face-based approach employs irregular three-dimensional grids with a generative faces number. The velocity flow field is computed using governing equations of momentum conservation, whereas the flow field of pressure is determined by deriving continuity and momentum equations into to the Bernoulli equation [11]. Additional fluid transport equations are discretized and evaluated according to the same principles as the Euler equation in turbulent flows. In Equation (1) and (2), which show the continuity and Euler equations, v is the flow speed, ∇ is the amount of mass moving, ρ is a fluid density, μ is a viscous stress, f is a force from the outside, and t is a time.

$$\frac{\partial \rho}{\partial t} + \nabla(\rho u) = 0 \tag{1}$$

$$\rho\left(\frac{\delta V}{\delta t} + v.\nabla v\right) = -\nabla p + \mu\nabla^2 v + f \tag{2}$$

RANS, which is based on the k-ω SST model, is utilized to model the near-wall turbulence phenomena [12]. The k-ω model has been shown to be more numerically stable than the k-ε model, particularly near the boundary layer of walls. This k-ω model, unlike other turbulent equation models, does not require damping functions due to the significant turbulent flow in the wall sections. In the wall boundary, the distance between the wall and the first point beyond the wall must be provided, numerically. Transport model equations, including the case of the k and ω turbulence levels, are provided in Equation (3) and (4), respectively.

$$\frac{\partial \rho K}{\partial t} + \frac{\partial}{\partial x_j}\left(\rho U_j K - (\mu + \sigma_k \mu_t)\frac{\partial K}{\partial x_j}\right) = \tau_{t_{ij}} S_{ij} - \beta^* \rho \omega K \tag{3}$$

$$\frac{\partial \rho\omega}{\partial t} + \frac{\partial}{\partial x_j}\left(\rho U_j \omega - (\mu + \sigma_k \mu_t)\frac{\partial \omega}{\partial x_j}\right) = \alpha \frac{\omega}{K}\tau_{t_{ij}} S_{ij} - \beta^* \rho \omega^2 \quad (4)$$

Where α = 5⁄9, β = 3⁄40, $\beta*$ = 9⁄100, σ = 0.5, $\sigma*$ = 0.5 following [9].

2.3 CFD modelling

It is imperative that the size of the domain is sufficient to prevent inaccurate simulation results. In an effort to better capture the wave effect around the model, the simulation domain did not employ the symmetry plane feature. Based on these factors, the configuration of the domain used in this study is two to three times larger than the ITTC recommendation (ITTC, 2011). The dimension of the domain is a function of the ship length model, represented by L, as shown in Figure 2. The velocity intake and pressure outlet borders are positioned 3L and 6L from the ship's front and rear ends, respectively. The expanded domain at the rear of the ship is determined to capture the contour of the free surface formed at the rear of the ship during its movement. In addition to the ship model, the top, side walls, and bottom are built as nonslip walls.

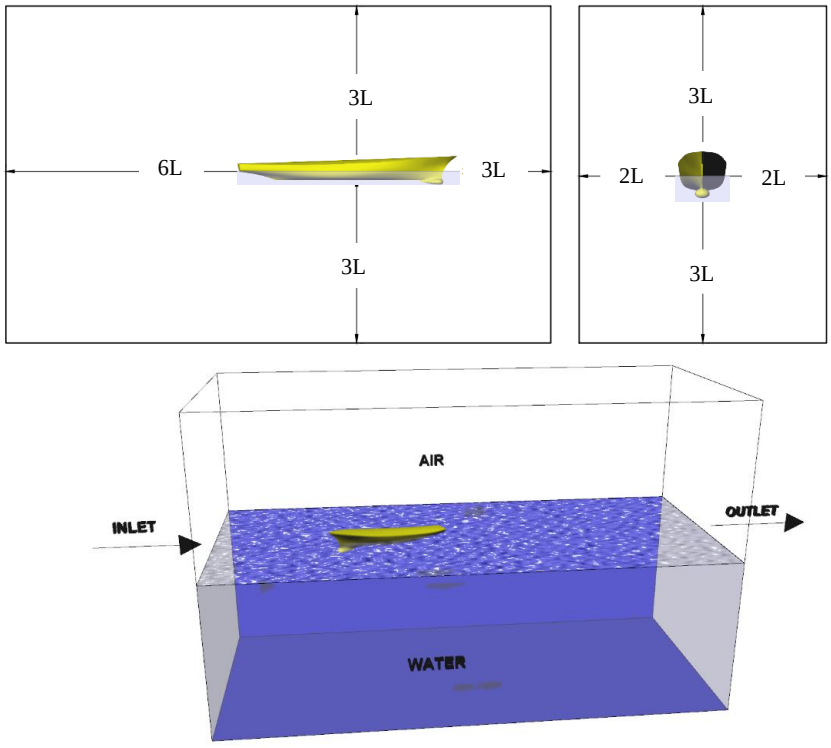

Fig. 2. Computational Domain and Boundary Conditions

The fluid flow occurring at the free surface area behind the ship, obtained by mesh refinement around the free surface and depicted in Figure 3, is an additional important representation. As its values are not further analyzed, the outer region is

left unrefined to conserve memory and reduce computational time. A structured hexahedral mesh is used to make the grid around this area to reduce the amount of computing work needed across the large computational domain. As depicted in Figure 3, a mesh deformation method is adopted to accommodate the heave and pitch motion, allowing the grid's structure to bend or deform without being torn when following the movement of the ship. This challenge is also overcome by enlarging the domain to accommodate free ship movements better. Figure 3 shows mesh deformation between 1 and 2 simulation seconds.

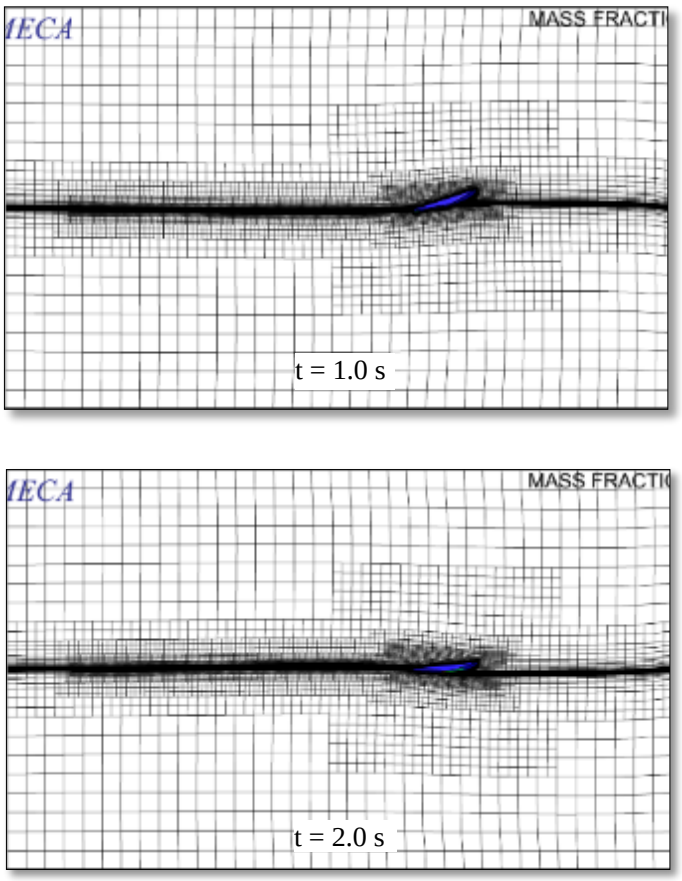

Fig. 3. Mesh deformation at t =1.0 s and 2.0 s

Grid independence testing is conducted at the Froude number of 0.28 on three parameters, namely the drag coefficient (C_T), heave motion, and pitch motion. Table 2 shows the number of grid independence study tests as well as the deviation between each test. The rate of change in the values of the three tested parameters helps visualize the results of the grid independence study test on the DTMB 5415 model. It is evident from Table 2 that the addition of the number of grids caused the tested results to change. The testing process can then be terminated if the difference between the before and after simulation steps is negligible, with the acceptable

maximum deviation decided to be no more than 2%. Based on the test results, it is determined that a grid containing approximately 1.5 million elements is sufficient for numerical simulations of the DTMB 5415 model. The deviation in the number of elements between simulation results is 0.77 percent of the C_T value, 1.01 percent of the heave motion value, and 0.5 percent of the pitch motion value, all below 2%.

Table 2. Results study of mesh independence on Model DTMB 5415

Mesh Numbers	Drag Coefficient (C_T)	Deviation C_T	Heave (mm)	Deviation Heave	Pitch (deg)	Deviation Pitch
187436	4.81×10^{-3}		-11.289		-0.1136	
374872	4.60×10^{-3}	4.35%	-10.713	5.10%	-0.1080	4.89%
749743	4.42×10^{-3}	3.98%	-10.370	3.20%	-0.1053	2.55%
1499485	4.38×10^{-3}	0.84%	-10.244	1.22%	-0.1041	1.12%
2998970	4.35×10^{-3}	0.77%	-10.141	1.01%	-0.1036	0.51%

2.4 Centre of gravity and radius of gyration

In this study, CFD simulation activates both heave and pitch motion degrees of freedom. It is crucial to determine the center point of gravity and the radius of gyration, as they influence the simulation results. For the purpose of calculating the radius of gyration, the three-dimensional model of DTMB 5415 is subdivided into twelve parts. The weight and center of gravity of each of these parts are then used to determine the radius of gyration. Using the reference [13], the radius of gyration k_{xx}, k_{yy}, and k_{zz} are calculated. Table 3 gives details about the radius of gyration and mass moment of inertia of the DTMB 5415 model in the CFD simulation.

Table 3. Radius of gyration and inertia mass moment of DTMB 5415.

Item	Value	Unit
k_{xx}	0.2950	m
k_{yy}	1.6615	m
k_{zz}	1.6646	m
k_{xx}/B	35.67	%
k_{yy}/LOA	26.92	%
k_{zz}/LOA	26.97	%
Displacement	554.15	kg
I_{xx}	48.23	$kg.m^2$
I_{yy}	1529.78	$kg.m^2$
I_{zz}	1535.50	$kg.m^2$

3 Result and Discussion

Numerical simulations essentially estimate the forces acting on the DTMB 5415 vessel which include drag and lift forces acting on the surface of the hull. These forces are hydrodynamic parameters that are considered in designing ships because they affect the hydrodynamic performance of the ship. The CFD simulation is carried out at the same speed as the ship model test, namely with three speed variations or Froude number values of 0.10, 0.28, and 0.41. The computational results obtained are then contrasted with the test finding of the DTMB 5415 ship model on the towing tank that has been published by ITTC. There are three parameters that are important to compare including the drag force or resistance of the ship, the motions of the heave, and the pitch which represents the lift force exerted on the ship. The results of the comparison between CFD simulation and experimental testing can be seen in Table 4, 5, and 6.

Table 4. Comparison results of drag coefficient between CFD simulation and model test.

Speed (Fn)	Drag Coefficient (C_T)		
	CFD	Model Test	Deviation
0.100	4.13×10^{-3}	3.98×10^{-3}	3.79%
0.280	4.38×10^{-3}	4.21×10^{-3}	4.01%
0.410	6.65×10^{-3}	6.50×10^{-3}	2.28%

Table 5. Comparison results of heave between CFD simulation and model test.

Speed (Fn)	Heave (mm)		
	CFD	Model Test	Deviation
0.100	-1.147	-1.050	9.28%
0.280	-10.244	-10.210	0.33%
0.410	-25.592	-25.340	0.99%

Table 6. Comparison results of pitch between CFD simulation and model test.

Speed (Fn)	Pitch (deg)		
	CFD	Model Test	Deviation
0.100	-0.014	-0.013	7.25%
0.280	-0.104	-0.104	0.12%
0.410	0.379	0.379	0.07%

Tables 4, 5, and 6 respectively demonstrate the amount of the discrepancy between CFD simulation results and model test results against the Coefficient Drag (C_T) values with an average of 3.36%, heave motion elevation of 3.53%, and pitch

motion elevation of 2.48%. Table 5 and 6 presents the highest value of deviation between the numerical and model test results for heave and pitch motions that occurred for Froude numbers of 0.1 about 9.28% and 7.25%, respectively. However, the three parameters provide an average difference of less than 4% so it can be concluded that the CFD results are quite representative of the test results. The wave making contours formed of the CFD simulation can be seen in Figure 5. The wave pattern around the ship's hull is generated due to the ship's forward motion, and the height of the generated waves increases as the ship's velocity increases. The generated wave at the stern is greater than the wave at the bow, and the difference between the two has grown as the ship's speed has increased. In addition, the width of the divergent wave and the length of the transverse wave grow as the ship's speed increases.

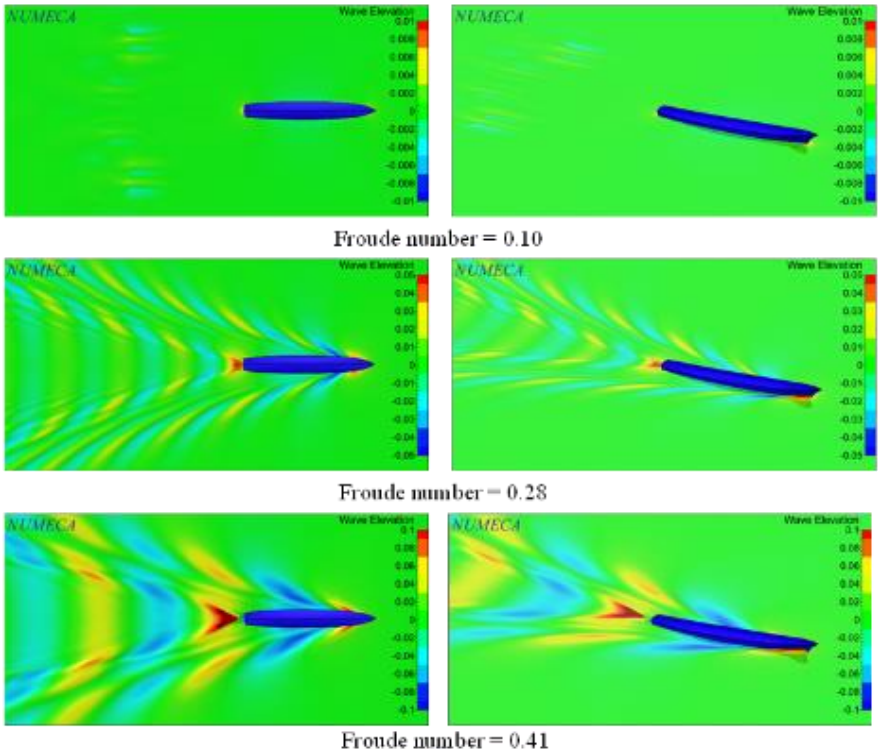

Fig. 5. Free surface contour of DTMB 5414 in Fr = 0.1, 0.28, and 0.28

Moreover, comparisons are made between the water surface contours generated by the CFD simulation and those of the laboratory model test [14]. Figure 6 displays a comparison of wake contours surrounding the body hull for Froude values of 0.28 and 0.41 based on the results of the CFD simulation and model test. At Froude number 0.1, there is no comparison because the water surface contours are so minute that they are nearly invisible. The similarity of the isoline in Figure 6 indicates that the results of the CFD simulation are very close to those of the model test. Isolines are lines that illustrate how the wave surface height varies with altitude.

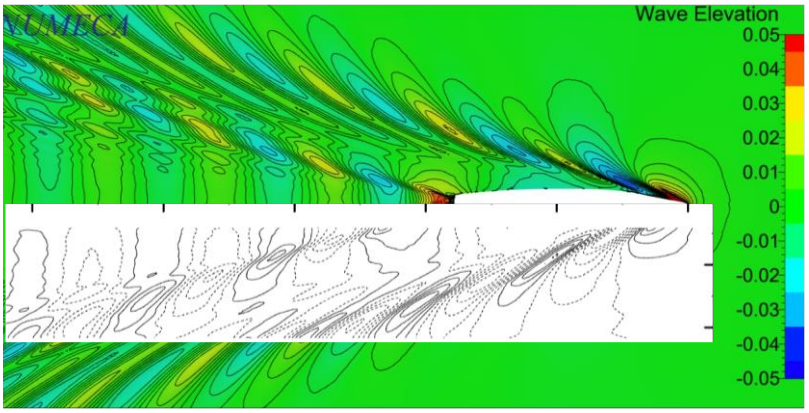

Froude number = 0.28

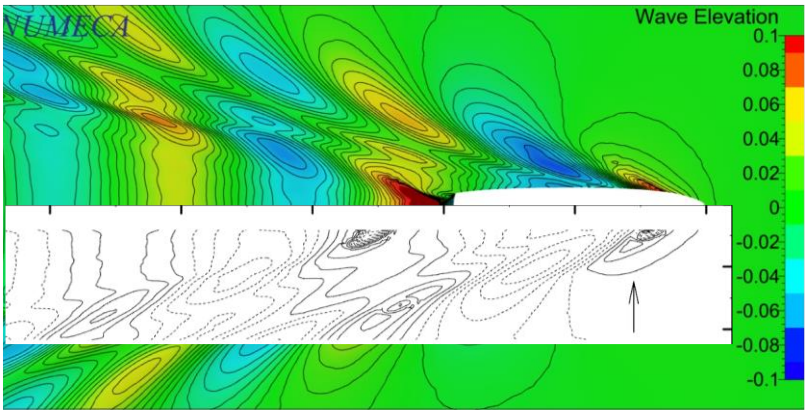

Froude number = 0.41

Fig. 6. Comparison of wave pattern between CFD simulation and Model test

Figures 7, 8, and 9 explains time history simulation for resistance force, heave motion, and pitch motion at various Froude number of 0.1, 0.28, and 0.41. All figures show that the high elevation always occurred at early time step up to around 10 second, and after that the response elevation is quite stable. The resistance force, heave motion, and pitch motion are taken as ship performance data after 10 seconds of simulation which is in stable conditions. The time history presented in Figures 7, 8, and 9 also convinces us that the elevation of heave and pith motion becomes higher linearly with increasing the ship's velocity. However, the heave and pitch motions are negligible because the lift force that occurred is negligible compared to the weighting force. In this study, there is no excitation force from regular waves acting on the hull, so the heave and pitch motions are caused by the lift force. As shown in Figure 7, the lift force is greater than the drag force, and the difference between the two forces decreases as the speed increases. With a high Froud number of 0.41, the lift force fluctuates significantly.

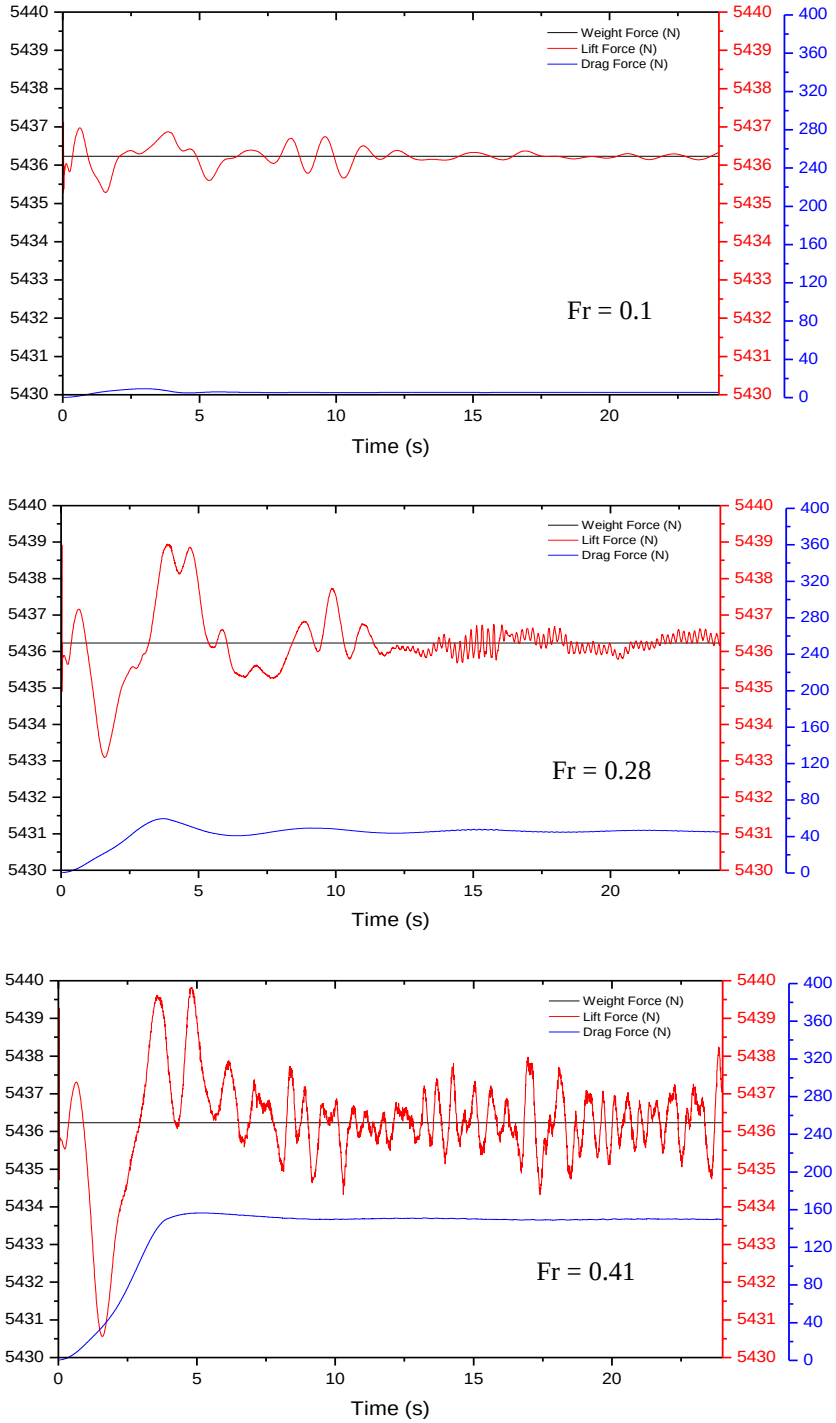

Fig. 7. Time history of forces in CFD simulation at Fr = 0.1, 0.28, and 0.41

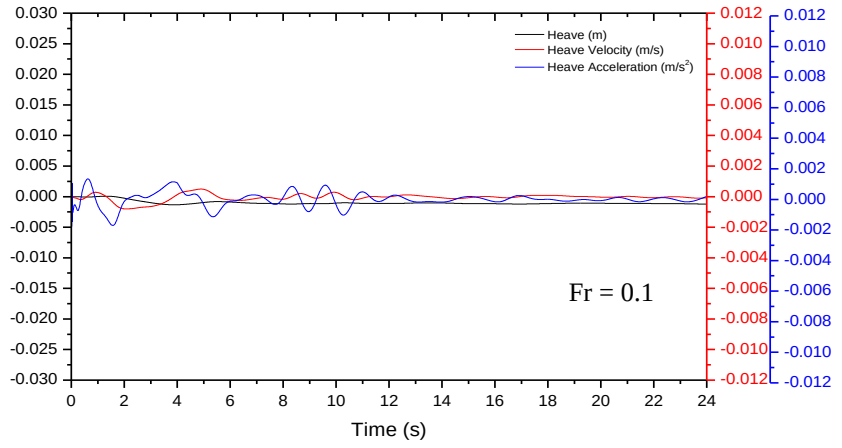

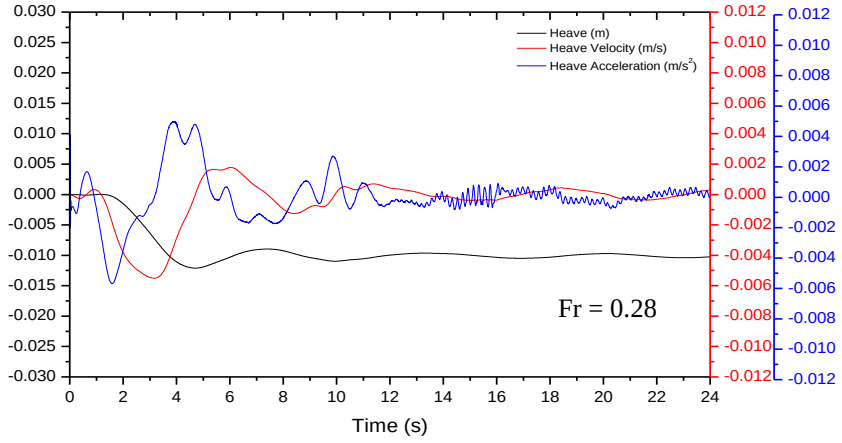

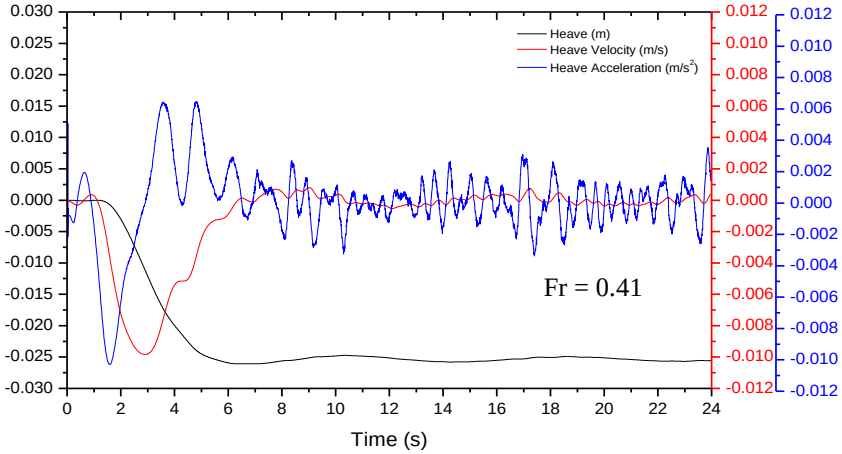

Fig. 8. Time history of heave motion in CFD simulation at Fr = 0.1, 0.28, and 0.41

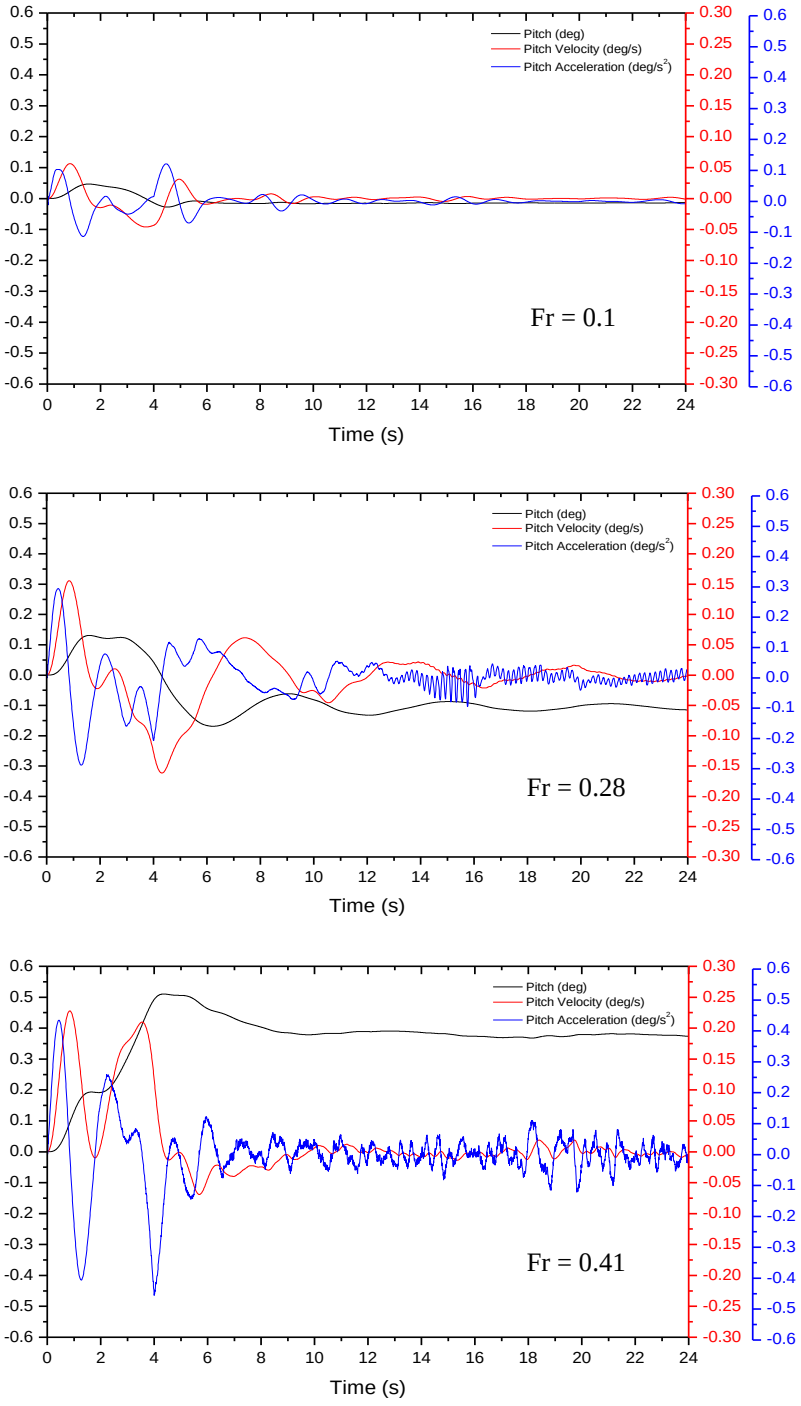

Fig. 9. Time history of pitch motion in CFD simulation at Fr = 0.1, 0.28, and 0.41

4 Conclusions

The NUMECA code has been utilized simulating free surface of turbulent flow model over the wetted surface hull of the DTMB 5415 model at three Froude numbers. The usage of a hybrid mesh in modeling under the RANS algorithm is highly advantageous when computational resources are restricted. The real fluid flow approach is utilized to evaluate the frictional and viscous pressure resistances of the model. The wake profile generated by the ship model as depicted by simulation compares satisfactorily with model test results for Froude number of 0.28 and 0.41. Furthermore, the total resistance results of the numerical simulation are extremely close to those of the published model test, with errors of 3.79 %, 4.01 %, and 2.28 % at Fr = 0.10, 0.28, and 0.41, respectively.

Acknowledgements

The authors are grateful to Badan Riset and Inovasi Nasional (BRIN) for providing funding under the scheme for basic research.

References

[1] Söding, H., Shigunov, V., Schellin, T.E., Moctar, O.E.: A rankine panel method for added resistance of ships in waves. Journal of Offshore Mechanic Arctic Engineering, vol. 136, no. 3, pp. 031601 (2014)

[2] Wackers, J., Koren, B., Raven, H.C., Ploeg, A.V.D., Starke, A.R., Deng, G.B., Queutey, P., Visonneau, M., Hino, T., Ohashi, K.: Free-surface viscous flow solution methods for ship hydrodynamics. Archives of Computational Methods in Engineering, vol. 18, pp. 1–41 (2011)

[3] Dawson, C.W.: A practical computer method for solving ship wave problems. Proceedings of the 2nd International Conference on Numerical Ship Hydrodynamics, Berkeley, CA, pp. 30–38 (1977)

[4] Belibassakis, K.A., Kegkeroglou, A.: A nonlinear BEM for the ship wave-resistance problem. Chapter book, Sustainable Development and Innovations in Marine Technologies book, London (2019)

[5] Hadian, M.R., Zarrati, A.R.: Application of Multi-Block method for simulating shallow free surface flows in complex geometries. Journal of Hydraulic Research, vol. 46, no. 5, pp. 668–678 (2008)

[6] Li, T., Matusiak, J.: Simulation of modern surface ships with a wetted transom in a viscous flow. Proceedings of the 11th International Offshore and Polar Engineering Conference, vol. 4, pp. 570–576 (2001)

[7] Ahmed, Y.M.: Numerical simulation for the free surface flow around a complex ship hull form at different Froude numbers. Alexandria Engineering Journal, vol. 50, pp. 229–235, (2011)

[8] Sulisetyono, A., Fadhlurrohman, I., Ali, B., Zubaydi, A.: Computational prediction of the resistance of the the floatplane at various trim angles, Journal of Theoretical and Applied Mechanics, vol. 60, no. 2, pp. 267–278 (2022)

[9] Aliffrananda, M.H.N., Sulisetyono, A., Hermawan, Y.A., Zubaydi, A.: Numerical analysis of floatplane porpoising instability at calm water during take-off. International Journal Technology, vol. 13, no. 1, pp. 190-201 (2022)

[10] ITTC: Resistance Committee: Final report and recommendation to the 27th ITTC. 27th ITTC Conference, Copenhagen (2014)

[11] Versteeg, H.K, Malalasekera, W.: An Introduction to computational fluid dynamics,

The Finite Volume Method book, Harlow: Pearson Education Limited (2007)
[12] Wilcox, D. C.: Reassessment of the scale-determining equation for advanced turbulence models, AIAA Journal vol. 26, pp.1299-1310 (1988)
[13] Bhattacharya, R.: Dynamic of marine vehicle. Marryland U.S. Naval Academy, Annapolis (1978)
[14] Olivieri, A., Pistani, F., Avanzini, A., Penma, R.: Towing tank experiments of resistance, sinkage and trim, boundary layer, and free surface flow around a naval combatant Insean 2340 Model, The Univeristy of Iowa, College of Engineering, IHRR-Hydro science & Engineering (2001)